

Dynamic Three-dimensional Simulation of Surface Charging on Rotating Asteroids

RONGHUI QUAN ¹, ZHIYING SONG ^{1,*} AND ZHIGUI LIU ¹

¹College of Astronautics, Nanjing University of Aeronautics and Astronautics, Nanjing, Jiangsu, 210016, China

ABSTRACT

Surface charging phenomenon of asteroids, mainly resulting from solar wind plasma and solar radiation, has been studied extensively. However, the influence of asteroid's rotation on surface charging has yet to be fully understood. Here neural network is established to replace numerical integration, improving the efficiency of dynamic three-dimensional simulation. We implement simulation of rotating asteroids and surrounding plasma environment under different conditions, including quiet solar wind and solar storms, various minerals on asteroid's surface also be considered. Results show that under typical solar wind, the maximum and minimum potential of asteroids will gradually decrease with their increasing periods, especially when solar wind is obliquely incident. For asteroid has period longer than one week, this decreasing trend will become extremely slow. During solar storm passing, solar wind plasma changes sharply, the susceptibility of asteroid's surface potential to rotation is greatly pronounced. Minerals on surface also count, plagioclase is the most sensitive mineral among those we explored, while ilmenite seems indifferent to changes in rotation periods. Understanding the surface charging of asteroid under various rotation periods or angles, is crucial for further research into solar wind plasma and asteroid's surface dust motion, providing a reference for safe landing exploration of asteroids.

Keywords: Asteroid rotation(2211) — Asteroid surfaces(2209) — Solar wind(1534) — Neural networks(1933)

1. INTRODUCTION

Small airless bodies such as comets and asteroids exposed to solar wind plasma and ultraviolet irradiation, are very sensitive to changes in surrounding magnetic and electric fields. Their exhibit surface charging phenomenon, caused by photoelectric effect, electron together with ion attachment and secondary electron emission, will react on surrounding plasma, changing the density distribution and temperature of electrons and ions. Therefore, when an asteroid has rotational velocity, day-night alternation always exists, the equilibrium of interaction between asteroids and surrounding plasma will be constantly reconstructed, efficient dynamic analysis of surface charging is necessary.

Surface charging of asteroids belongs to the field of interaction between solar wind and asteroids. Researches in this direction can be roughly divided into three categories: electrification properties and electrostatic driving dynamics of surface dust particles, overall charging properties of asteroid surfaces, and deep charging of asteroids induced by surface charging. Existing researches center on the charged properties (Zimmerman et al. 2016; Oudayer et al. 2019) and floating motion (Hartzell & Scheeres 2012) of regolith grains on the surface, mostly using magnetohydrodynamic (MHD) or hybrid particle-in-cell (Hybrid PIC) model. Here we focus on the second category. At the terminator between night and day, the maximum electric field strength appears, almost 10 times that of dayside (Xie et al. 2023), in this region, electron temperature is the most important parameter (Stubbs et al. 2014). On the dayside of asteroid, photoelectron current usually dominates, surface potential is always positive, theoretical possibilities have been discussed (Kureshi et al. 2020). Correspondingly, on the night side, charging current mainly comes from the incidence of electrons and ions in solar wind plasma, the surface presents a negative potential, during solar energetic particle (SEP) events, this negative potential may reach thousands (Halekas et al. 2007). However, if enough secondary electrons are emitted, potential of night side can sometimes become positive.

* Correspondence to: Zhiying Song, sx2215054@nuaa.edu.cn

While the theoretical foundation of surface charging is relatively solid, static simulations of asteroids at specific angles are also feasible, how to dynamically model and verify the surface potential of asteroids with rotation remains an urgent problem to be solved. Operating traditional modeling techniques for three-dimensional simulation means that after asteroid rotates a certain angle, surrounding environment and surface potential of the entire asteroid need to be recalculated through integration and solving ordinary differential equations, resulting in a significant rise in computational complexity, analysis of potential under different rotation periods will be extremely challenging.

In this paper, neural network is used to calculate surface potential of asteroid under given solar wind and material parameters rather than numerical calculation, which is adopt to form the training dataset, greatly improving the efficiency of real-time analysis. We use COMSOL Multiphysics to perform multi-scale modeling simulation, namely divide the whole simulation area with a radius of 500 m into several scales, adopt the smallest scale, i.e. the highest accuracy for the region around asteroid, then increase simulation scale for external plasma, thereby reducing computational complexity. We set three major conditions in order to comprehensively analyze how rotation of asteroids affect their charging properties. Specifically, we first explore asteroids exposed to typical solar wind with fixed surface material, rotation periods from 1 hour to half a year are all considered. Then solar storm is taken into consideration. A coronal mass ejection (CME) existing in early May, 1998 product rapid changes in solar wind density and temperature, four stages of this event have their distinct characteristics, further make vastly separated potential. Due to the complex surface composition of asteroids, it is necessary to explore the charging properties of different minerals, plagioclase, orthopyroxene and ilmenite were studied.

Specific surface charging mechanism and composition of the current balance equation are introduced in Section 2, including photoelectron current, incident electron and ion current, secondary electron current, backscattered current, and conduction current in a thin range of asteroid's surface. How surface potential react on surrounding plasma will also be described in this Section. Establishment of model and parameter settings are shown in Section 3. Comparison and analysis of simulation results are present in Section 4. Finally, we summarize our work in Section 5.

2. MECHANISM OF SURFACE CHARGING

2.1. Current balance equation

The current balance equation is the basis of charging theory, surface potential attribute to the accumulation of surface charges, caused by interaction between asteroid and space environment. It is feasible to construct the equilibrium equation in the case of treating a thin area on the surface of asteroid as a dielectric (Xin-Yue et al. 2016).

The current balance equation can be expressed as following:

$$C \frac{dU}{dt} = -J_e + J_i + J_{se} + J_{si} + J_{ph} + J_{bse} - J_c \quad (1)$$

where U is instantaneous surface potential of asteroid, C is equivalent capacitance, determined by relative permittivity ϵ_r . J_e and J_i are environmentally induced electron and ion current density, respectively, J_{se} and J_{si} are secondary emitted electron current density caused by electron and ion, J_{ph} is photoelectron current density, J_{bse} is backscattered electron current density, and J_c is conduction current density.

In order to solve Equation (1), necessary expressions of each current density are presented below.

1. Photoelectron current emitted from asteroid is a function composed of locational material, solar radiation flux $S(E)$, and electron yield of a single photon $W(E)$ (Hastings & Garrett 2004). For surfaces with zero or negative potential, photoelectrons will successfully escape, creating initial photoelectron current density:

$$J_{ph0} = \int_{W_0}^{\infty} W(E)S(E)dE \quad (2)$$

where W_0 is work function.

Considering that positive surface potential hinders the overflow of photoelectrons, the expression for photoelectron current can be revised to:

$$J_{ph} = \begin{cases} J_{ph0}, U \leq 0 \\ J_{ph0} \exp\left(\frac{-eU}{kT_{ph}}\right) \left(1 + \frac{eU}{kT_{ph}}\right), U > 0 \end{cases} \quad (3)$$

where e is the unit charge, k is Boltzmann constant, T_{ph} is photoelectron temperature, which equals 2.2eV in this paper.

2. Assuming that both electrons and ions follow bi-Maxwellian distribution (Novikov et al. 2008), when surface potential $U \leq 0$, only the fraction of electron with $E \geq eU$ can arrive the surface (Wang et al. 2016), that means the original energy of electron corresponds to $E - eU$. Therefore, incident electron current density is (Whipple 1981):

$$J_e = \begin{cases} \sum_{j=1}^2 e n_{e,j} \left(\frac{kT_{e,j}}{2\pi m_e} \right)^{\frac{1}{2}} \exp\left(\frac{-eU}{kT_{e,j}}\right), U \leq 0 \\ \sum_{j=1}^2 e n_{e,j} \left(\frac{kT_{e,j}}{2\pi m_e} \right)^{\frac{1}{2}} \left(1 + \frac{eU}{kT_{e,j}} \right), U > 0 \end{cases} \quad (4)$$

where n_e is electron density, T_e is electron temperature, m_e is Electron Mass.

In the similar manner, incident ion current density can be described as:

$$J_i = \begin{cases} \sum_{j=1}^2 q_i n_{i,j} \left(\frac{kT_{i,j}}{2\pi m_i} \right)^{\frac{1}{2}} \left(1 + \frac{q_i U}{kT_{i,j}} \right), U \leq 0 \\ \sum_{j=1}^2 q_i n_{i,j} \left(\frac{kT_{i,j}}{2\pi m_i} \right)^{\frac{1}{2}} \exp\left(\frac{-q_i U}{kT_{i,j}}\right), U > 0 \end{cases} \quad (5)$$

where q_i is ionic charge, n_i is ion density, T_i is ion temperature, m_i is ion mass.

3. Secondary electron current density due to electrons is represented as the product of secondary electron yield and incident electron current density:

$$J_{se} = \begin{cases} Y_{se}(E) J_e, U \leq 0 \\ Y_{se}(E + eU) J_e, U > 0 \end{cases} \quad (6)$$

That due to ions is in the same form:

$$J_{si} = \begin{cases} Y_{si}(E - eU) J_i, U \leq 0 \\ Y_{si}(E) J_i, U > 0 \end{cases} \quad (7)$$

Backscatter current is the current generated by surface scattering of incident electrons, which is determined by backscattered electron yield of the surface material:

$$J_{be} = \begin{cases} Y_{be}(E) J_e, U \leq 0 \\ Y_{be}(E + eU) J_e, U > 0 \end{cases} \quad (8)$$

where Y_{se} and Y_{si} are secondary electron yield induced by electrons and ions respectively, Y_{be} is backscattered electron yield, their formulas are adopted according to reference (Pandya et al. 2019).

4. Conduction current represents the current conducted from the surface of equivalent dielectric to the back:

$$J_c = \frac{U}{\rho d} \quad (9)$$

where ρ is conductivity, d is the thickness of dielectric, here it equals 0.01mm.

2.2. Interaction with Solar Wind Plasma

When surface charging appears, electric field is formed around the asteroid, electrons and ions will move under the traction of electric field force, drift-diffusion equations (Gorin et al. 2020) are widely used to solve these problems of plasma physics.

$$\begin{cases} \frac{\partial n_e}{\partial t} + \nabla \cdot \mathbf{\Gamma}_e = R_e - (\mathbf{u} \cdot \nabla) n_e \\ \mathbf{\Gamma}_e = -\mu_e \mathbf{E} n_e - D_e \nabla n_e \end{cases} \quad (10)$$

where R_e is electron generation rate, $\mathbf{\Gamma}_e$ is the related flux-density vector, \mathbf{u} is the velocity vector, μ_e and D_e are the mobility and the diffusion coefficient of electrons, satisfy Einstein relation, can be represented as:

$$\begin{cases} \mu_e = \frac{e}{m_e v_{ce}} \\ D_e = \frac{kT_e}{m_e v_{ce}} \end{cases} \quad (11)$$

where v_{ce} is the frequency of electron-neutral collisions, can be derived from kinetic theory of plasma (Gurevich 1978; Ginzburg 1970).

Representing the frequency of ion-neutral collisions with v_{ci} , the mobility and the diffusion coefficient of ions can be expressed analogously:

$$\begin{cases} \mu_i = \frac{q_i}{m_i v_{ci}} \\ D_i = \frac{kT_i}{m_i v_{ci}} \end{cases} \quad (12)$$

Changes in surrounding plasma, especially density and temperature of electrons and ions, will alter surface potential of asteroid, then modify electric field distribution in this area, causing the plasma to undergo changes again, forming a cycle. During this process, the rotation of asteroid and day-night alternation on the surface will greatly affect the equilibrium value. Therefore, to accurately analyze surface charging phenomenon, previous static analysis is insufficient, we need to dynamically simulate the asteroid and surrounding plasma.

3. MODEL DESCRIPTION

3.1. Neural Network

Substitute solar wind and material parameters into the current balance equation, it can transform into an ordinary differential equation solely related to potential. Potentials obtained from solving this equation, along with the parameters, will build a dataset to train a BP (Back Propagation) neural network (Quan et al. 2023), for the reason that achieve fast and accurate calculation of surface potential in subsequent dynamic simulation.

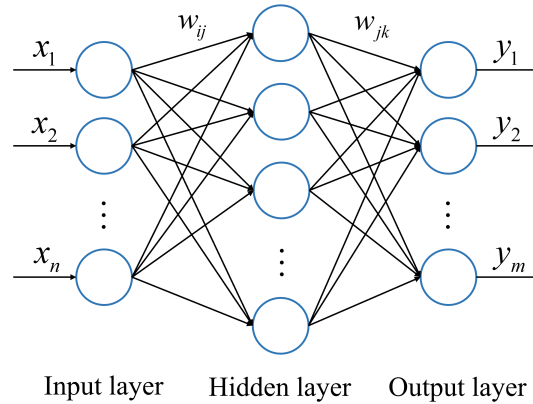


Figure 1. Structure of BP neural network. x_i represents input data while y_i represents output data. w_{ij} and w_{jk} mean neurons' weights, the goal of training is to update them then minimize the loss function.

BP neural network is a multi-layer feedforward network trained by error inverse propagation algorithm (Hu & Changliang 2018). Its topology, as shown in Figure 1, can be divided into three levels: input layer, hidden layer, and output layer. Take mean square error (MSE) as standard, by learning the input-output dataset with steepest gradient descent method, through reverse propagation to continuously adjust weights of each layer, in an effort to minimize errors, it can structure and store massive mapping relationships hidden under a big dataset, owning excellent generalization ability and strong fault tolerance (Liu et al. 2022).

All input and output parameters selected are present in Table 1. In this paper, two neural networks are trained, in order to calculate instantaneous potential and equilibrium potential, respectively. The former is applied to situations where the time step is less than 1s, mainly for the beginning of simulation. When the period is long enough to make time step reaches more than 1s, much higher than the time needed for surface to reach equilibrium potential, we can use equilibrium potential for calculation.

Before training, data normalization is considered, eliminate differences in order of magnitude between parameters, thus avoid unnecessary network errors. ReLU is used as activation function, it can compensate for the problem of Vanishing Gradient that Sigmoid and Tanh have, helping network learn complex patterns in data.

Table 1. Parameters of neural network

		Electron density
		Ion density
	Solar wind plasma	Electron temperature
		Ion temperature
		Solar radiation
Input		Work function
		Maximum secondary electron yield
	Material	Energy for maximum secondary electron yield
		Relative permittivity
		Conductivity
		Current potential (instantaneous only)
		Time step (instantaneous only)
Output		Potential at the next moment (instantaneous)
		Equilibrium potential(equilibrium)

3.2. Dynamical Multi-scale Model

A three-dimensional model has been developed to investigate surface charging phenomenon in solar wind plasma, we use COMSOL Multiphysics to realize the simulation. COMSOL is a universal software platform used for modeling and simulating physical field problems. It is based on finite element analysis, capable of exploring real physical phenomena by simulating a single physical field and flexibly coupling multiple physical fields.

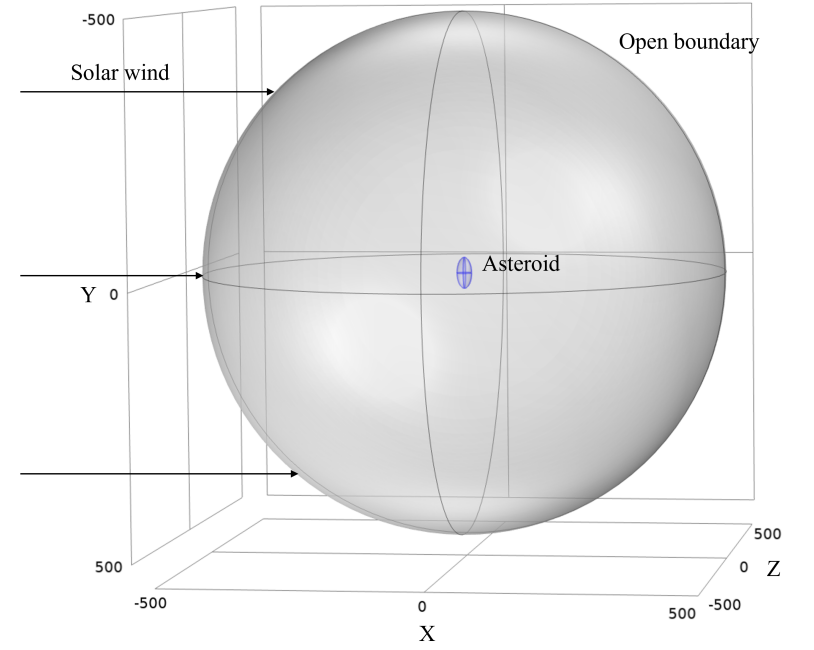


Figure 2. The schematic diagram of the simulation geometries. The gray cylinder indicates our simulation domain and the blue ellipsoid represents asteroid. The three black arrows on the left show the direction of solar wind.

We use the shape of 2016HO3 with a width-to-length ratio smaller than 0.48 to represent asteroid, regard it as a triaxial ellipsoid with semi-major axis of 29.5, 14, 14m (Li & Scheeres 2021). As indicated in Figure 2, the simulation domain is a sphere with a radius of 500m, asteroid locates at the center of it, the Z-axis is antiparallel to the spin axis of asteroid.

Our studies can be summarized as the following steps:

- a. Input plenty of solar wind parameters and material parameters, compute instantaneous and equilibrium potentials on asteroid's surface under these conditions with numerical integration, thereby build a dataset.
 - b. Divide the dataset into training and testing sets, train and optimize neural network.
 - c. Model asteroid within a simulation domain in Figure 2, initialize electrostatic field of asteroid's surface and surrounding plasma.
 - d. Input parameters (including solar wind plasma, solar irradiation, and material) at various locations into neural network, then output surface potential.
 - e. Calculate potential and electric field distribution within the remaining domain.
 - f. Simulate drift-diffusion motion of electrons and ions, then compute surrounding density and temperature of them.
 - g. Update input parameters of neural network, output surface potential at the next simulation timestep.
 - h. Iterate steps d-g until reaches required duration (e.g., one rotation period of asteroid).
- This process is illustrated in Figure 3.

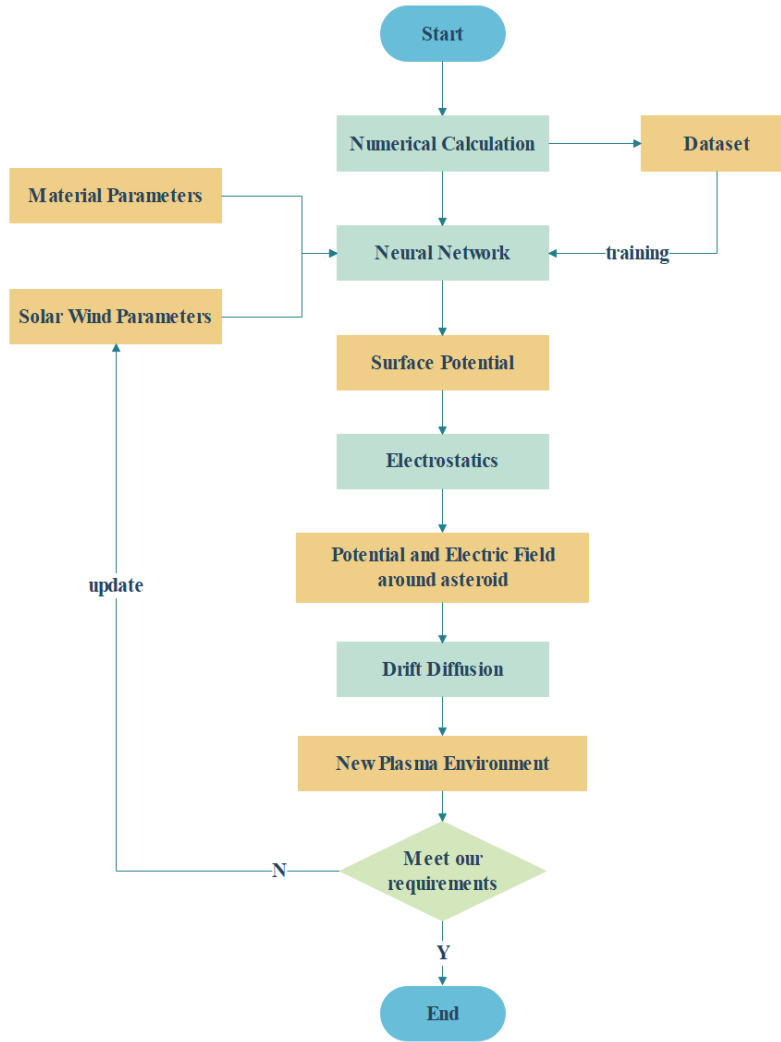


Figure 3. Flow chart of modeling and simulation. Numerical calculation only serves to build the dataset, it will not appear in subsequent simulations.

Operate parameters of PIC simulation (Xie et al. 2023) to verify our method, where $T_e = 10\text{eV}$, secondary electron yield has a peak yield of $\delta_{\max} = 1.0$ at the energy of $E_{\max} = 350\text{eV}$. solar wind parameters are at their typical values,

with number density of $5e6/m^3$, a velocity of 400km/s, time step is $1.0e-6s$, while the simulation period is 0.001s, the angle α between the major axis of asteroid and solar wind is fixed. Results are shown in Figure 4.

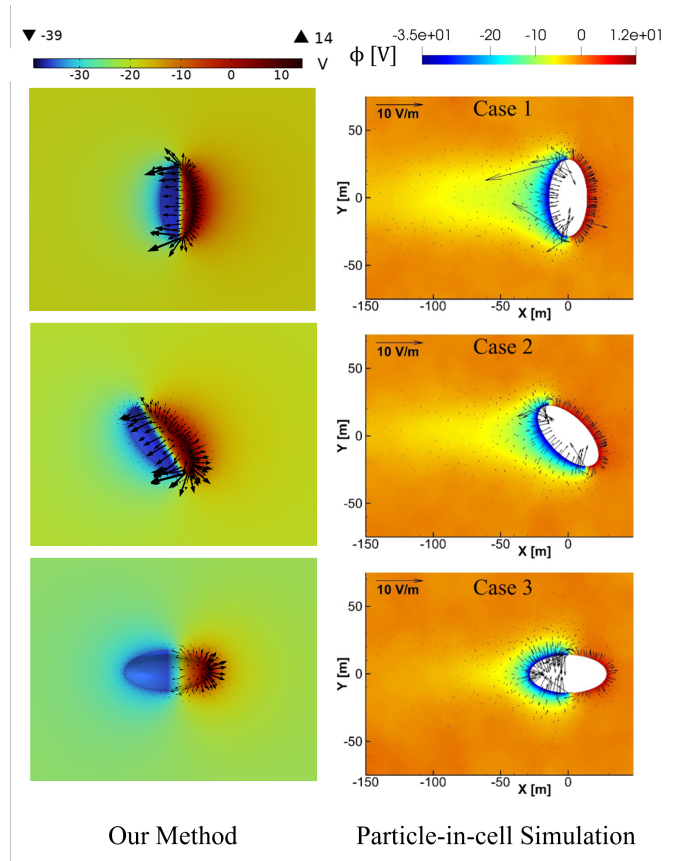


Figure 4. Comparison between our simulation method and PIC simulation. The three subfigures on the left shows results of multi-scale modeling simulation, indicating potential and electric field around asteroid. Those on the right are results from reference (Xie et al. 2023) under the same circumstances.

We can see a positive potential up to 13.6V on the dayside and a negative potential as low as -37.4V on the nightside when the angle $\alpha = 0^\circ$, while surface potential is +12V near the subsolar point, and -35V on the nightside with PIC simulation. It can be seen that our method is reliable.

Then we will conduct dynamic simulations asteroids about surface charging under different conditions, the three main categories are shown as follows:

(1) Surface Charging Properties of Rotating Asteroids under Normal Condition

Solar wind flows in the +X direction, number density is equal to $8e6/m^3$, electron temperature is 15eV while ion temperature is 10eV. Electrons and ions are emitted from the outer boundaries with a bulk speed of 400 km/s, an open boundary condition is applied here, where all particles can escape through the boundary. Small-scale mesh is used within 50 m around asteroid for fine simulation, as to the remaining areas, mesh adopt will scale up appropriately in line with standard of research.

Solar radiation received by surface depends on solar elevation angle, solar radiation reaches the peak at the subsolar point, then reduce gradually along with decreasing solar elevation angle till cross the terminator, solar radiation intensity thus become 0 on the night side. Plagioclase regards as material on the surface of asteroid, its work function is 5.58eV, threshold wavelength is 238nm. Secondary electron emission is taken into account here, with maximum secondary electron yield of 2.8 at the energy of 1000eV. The simulation period is set in accordance with rotation period, initial time step is $1e-5$ s, then become 1 s for asteroids have short rotation periods, such as 1 hour, finally grow to 1 hour when rotation period is half a year. However, no matter how long rotation period is, time step always much smaller than it, making it reasonable to analyze potential under various rotation angles.

(2) Impact of Rotation on Asteroids during the Passage of Solar Storm

On 29 April 1998, a CME emitting from the Sun was observed by The Lunar Prospector (LP) spacecraft, having a significant impact at Earth (Farrell et al. 2012). A forward shock occurred at 21 UT on May 1, followed by a clear CME, with counterstreaming electrons and a depressed proton temperature, then multiple shocks and CMEs appeared, finally came to an end at 1 UT on May 4 (Skoug et al. 1999). During the passage of CMEs, both density and temperature of solar wind will undergo drastic changes, even obtain values 10 times that in usual.

This entire series of events can be divided into four distinct temporal parts: typical solar wind; a dense, hot shock; early stage of CME; and late stage of CME (Zimmerman et al. 2012). Four simulation cases with their solar wind parameters have been performed in Table 2.

Table 2. Plasma parameters during passage of solar storm

Stage	Typical	Shock	Early CME	Late CME
Number density(/ cm^{-3})	5~8	20	3	≥ 50
Bulk speed(km/s)	400~450	600	650	500
T_e (eV)	15	80	9	16
T_i (eV)	10	40	6	4
c_s (km/s)	37.91	87.54	29.36	39.15

Surface mineral of asteroid is plagioclase, in terms of researches about charging properties, we set a rotation period of 0.467 hour in each case, equivalent to the spin period of 2016 HO3. In the discussion of how rotation period effect on surface charging, other periods are added.

(3) Differences between Asteroids with Various Surface Minerals

Except plagioclase, we studied orthopyroxene and ilmenite, obtain their charging results, then explore their sensitivity of surface potential to attitude of asteroids, their material parameters can be indicated in Table 3.

Table 3. Material properties of different minerals

Surface mineral	Work function(eV)	Threshold wavelength(nm)	δ_{\max} (eV)	E_{\max}
Plagioclase	5.58	238	2.8	1000
Orthopyroxene	5.14	259	2.1	700
Ilmenite	4.29	297	2.5	600

Solar wind parameters take that same as (1), rotation periods of asteroid are 1 hour, 6 hours and 1 day.

4. SIMULATION RESULTS

(1) Surface Charging Properties of Rotating Asteroids under Normal Condition

Surface potential of asteroids with eight rotation periods from 1 hour to half a year are simulated, even without solar storm, there can be macroscopic potential differences on surface of asteroids with different periods.

Figure 5 displays the surface potential of asteroid with three classical attitudes, as well as the distribution of electron density and ion density around it, the rotation period is always 1 day. Consistent with the results of static simulation, potential on the nightside is the lowest when $\alpha = 45^\circ$ compared with other two conditions. Meanwhile, if the main axis of asteroid is perpendicular to the direction of solar wind incidence, potential on the dayside is obviously higher than other situations.

As for the surrounding solar wind plasma, because of its much higher mobility and diffusion coefficient, electron responds more promptly to the electric field, has a relatively uniform distribution, there won't be exaggerated faults for density. Correspondingly, for ions primarily driven by the general flow of solar wind, will form a visible plasma wake at the tail of asteroid. As a result, during the rotation of asteroid, electron density undergoes significant changes with the surface charging conditions. Electrons entering the region will accumulate around asteroid, with a peak value up to $8e7/\text{m}^3$, 10 times the initial solar wind number density. At the same time, ion density will only fluctuate

within a small range, even cannot exceed $1e7/m^3$, and exhibits an extremely low value in the wake of asteroid. This phenomenon leads to differences in surface potential of asteroids during rotating.

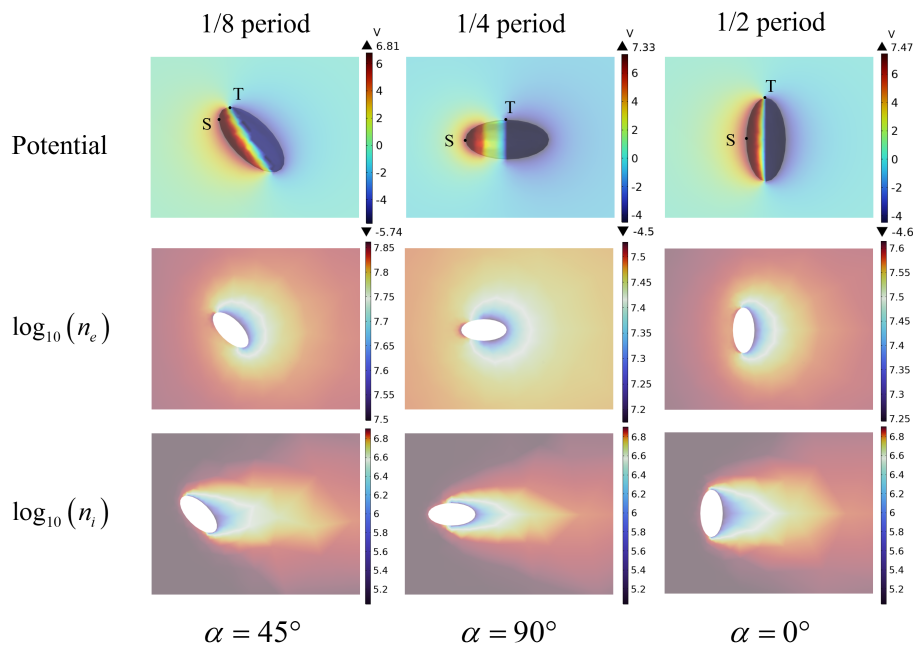


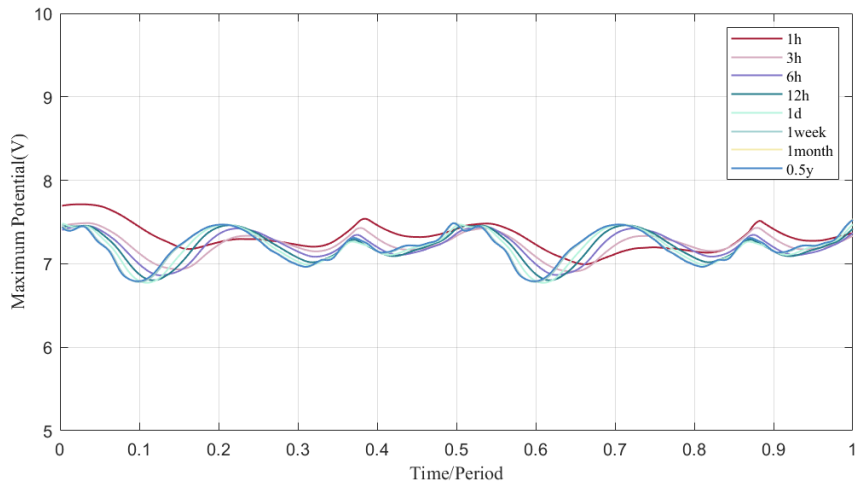
Figure 5. Surface potential and surrounding plasma of asteroid with rotation period of 1 day. Subfigures in the first row show surface potential of asteroid, points S and T locate at the subsolar point and the terminator. The other two rows represent densities of electrons and ions in the XY plane respectively.

The maximum and minimum potential on the surface of asteroid with different rotation periods are shown in Figure 6. Due to the fact that photoelectron current is the main source of surface charging on the dayside, potential here is less affected by fluctuations in electron and ion density compared to that on the nightside. The maximum potential always locates at the point of direct sunlight, appears much smoother and more stable than the minimum potential. However, their general downward trend with the growth of rotation period is still consistent.

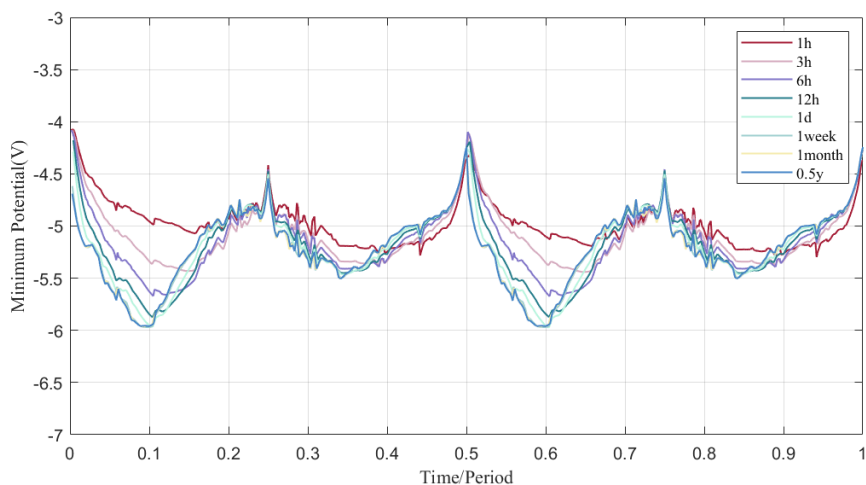
Asteroids with short rotation periods, such as 1 hour, have fast rotation angular speed, bring rapid alternation of illuminated face and shadowed face, along with electric field. Its ability to collect electrons is rather weak, potential has no clear valley value during rotation. Later, as the period increases, before reaching 1 week, the charge accumulation around asteroid will gradually become obvious. The peak value of average electron density in small-scale area will increase from $3.07e7/m^3$ at 1 hour to $7.60e7/m^3$ at 1 week, thus the minimum potential continues to decrease, in the meantime reduce the maximum potential. The range of potential can be changed from $+6.99V \sim +7.71V$ and $-5.30V \sim -4.07V$ at 1 hour to $+6.78V \sim +7.53V$ and $-5.97V \sim -4.24V$ at 1 week.

Apart from period, the direction and angle of rotation can also affect charging results, for example, $\alpha = 45^\circ$ and $\alpha = 135^\circ$ are the same situation for asteroids when we use static simulation, but considering that they are rotating, their results differ significantly. Besides, from Figure 6, we can conclude that no matter how long the period is, surface potential tends to be low when solar wind is obliquely incident, this phenomenon will become more obvious as rotation period increases. That's because when asteroid rotates to $\alpha = 25^\circ \sim 45^\circ$, the subsolar point S , where often has the maximum potential, is close to the terminator T . According to Poisson's Equation, the sudden change in potential over a short distance will strengthen electric field near asteroid, accelerate electrons to $2.21e7m/s$, the resulting higher electron density and electron temperature therefore reduce surface potential. This process continues until electric field and plasma reach a dynamic balance, which will be broken and reshaped after asteroid rotates through a large enough angle.

This explains why the curve of a short-period asteroid is rather stable: before surface potential falls low enough, asteroid and plasma must move toward a new balance. In this new situation, electric field is much softer, unable to prevent electrons from escaping due to density difference. In the same principle, asteroids with periods longer than 1



(a)



(b)

Figure 6. Potential under different rotation periods. (a) shows the maximum potential on the surface of asteroid within one rotation period, (b) shows the minimum potential.

week possess the capacity to attain equilibrium when solar wind is incident obliquely, -5.97V is the minimum potential asteroid can reach with these given parameters, it is also the potential that enables plasma and asteroid to become balanced when $\alpha = 36^\circ$.

(2) Impact of Rotation on Asteroids during the Passage of Solar Storm

Figures 7-8 show results from a simulation with the occurrence of CME. Five attitudes are selected for display, in regard to typical solar wind, the dayside always charged positively, its potential depends on solar elevation angle, will decrease apparently during the process from subsolar point to the terminator, until it turns into a small negative potential on the nightside. When the forward shock exists, solar wind number density and temperature experience a sharp increase, solar wind starts to accelerate. At this point, a sudden drop can be seen in surface potential, photoelectron current is inferior to the current generated by high-energy electrons, the dayside is charged negatively, such as the potential of -52V when $\alpha = 60^\circ$, the minimum potential on the nightside can reach -84.54V , close to 20 times that under normal circumstance, at this time, electron density here is $2.91\text{e}9/\text{m}^3$. Therefore, even though at the same angle, potential difference between parts of asteroid's surface can exceed 40V , contributing to exponential growth of electric field strength, as seen in Figure 8, electric field strength near asteroid, particularly the terminator, where there is a sharp transition between positive and negative potentials, has reached the level of $10\text{V}/\text{m}$, greatly

enhancing the sensitivity of electrons and ions to the charged properties of asteroid, plasma is extremely unstable, thus the surface potential curve performs strong volatility. It only takes 1/12 period to make the average electron density increase from $4.66e8/m^3$ to $7.26e8/m^3$, bring about a potential drop of more than 10V.

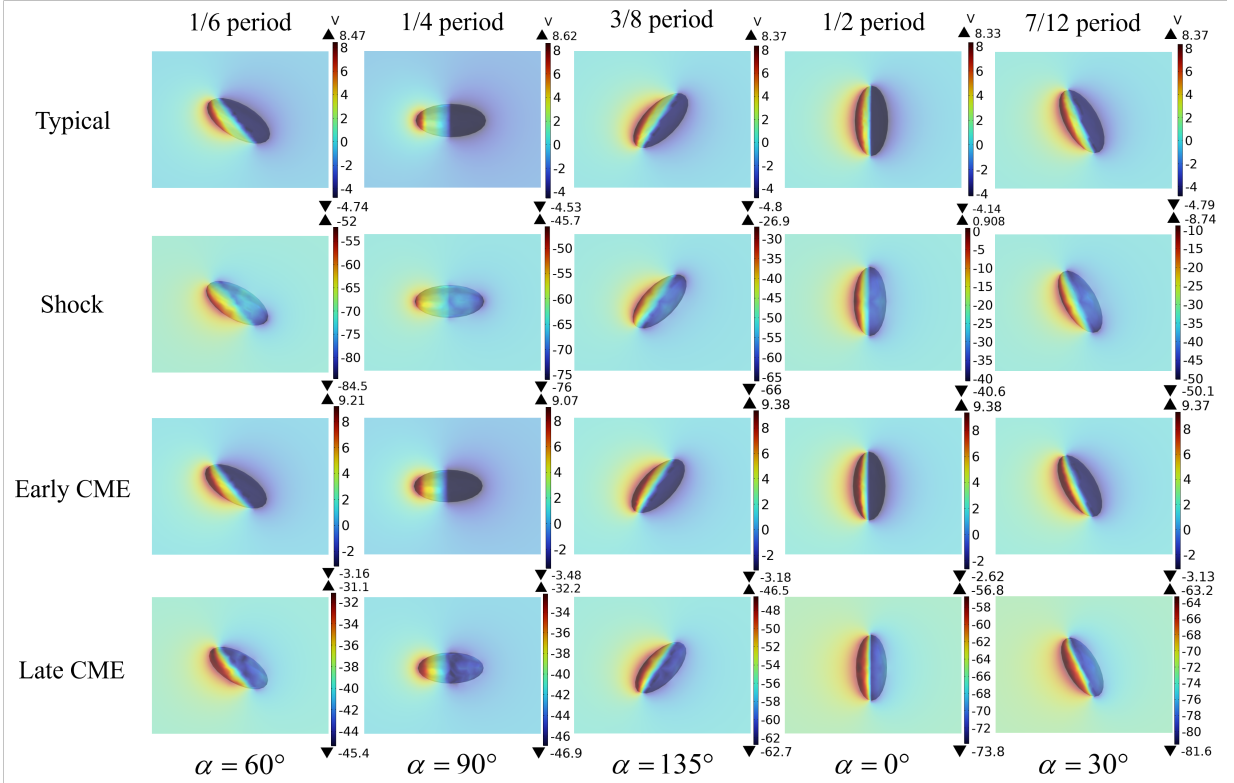


Figure 7. Simulated potential during passage of the modeled CME. α is the angle between solar wind and the major axis of asteroid, ranging from 0 to 180 degrees. $\alpha = 180^\circ/210^\circ$ is equivalent to $\alpha = 0^\circ/30^\circ$.

In addition to magnitude, the distribution of potential is also worth investigating. According to equation (11-12) and kinetic theory of plasma, both electrons and ions during shock achieve larger diffusion coefficients, the effect of drift-diffusion can partially overpower the flow of solar wind, increasing the density around asteroid's backside, then decrease surface potential there, allowing electrons to gather at the terminator, where has the strongest electric field. In contrast to the virtually uniform negative potential on the nightside during typical solar wind and early CME, potential during shock has a distinct gradient. In most cases, potential at the terminator is clearly lower than other parts, except $\alpha = 90^\circ$, when solar elevation angle declines most slowly on the dayside, reducing the potential difference near the terminator, thereby weakening the electric field. Because of the fast-flowing solar wind, ions produce a considerable wake near asteroid's tail, whereas high-temperature electrons do not. As a result, electron current far exceeds ion current, resulting in the lowest potential here.

The CME event has a lengthy duration, can be divided into early and late stages. Early CME exhibits characteristics of fast-flowing and cool, with a slightly lower number density than typical solar wind. Charging results at this stage have only minor differences from that of typical solar wind, in details, surface potential during early CME has a lift of $1\sim 2V$, mainly attributed to the low energy of charged particles. Photoelectron current on the dayside results in prominent positive potential. Furthermore, late CME produces more interesting phenomenon, the dense plasma flows slowly, surface of asteroid shrouded in it always has extreme negative potential, since electric field strength is not enhanced like that in shock, asteroid during late CME has more uniform surface potential. It is worth noting that surface potential will not reach its peak as in the former three stages, but it will continue to decrease. This is because for dense plasma, the equilibrium potential often needs to be several hundred volts, short-period asteroid is unable to reach this level within one period.

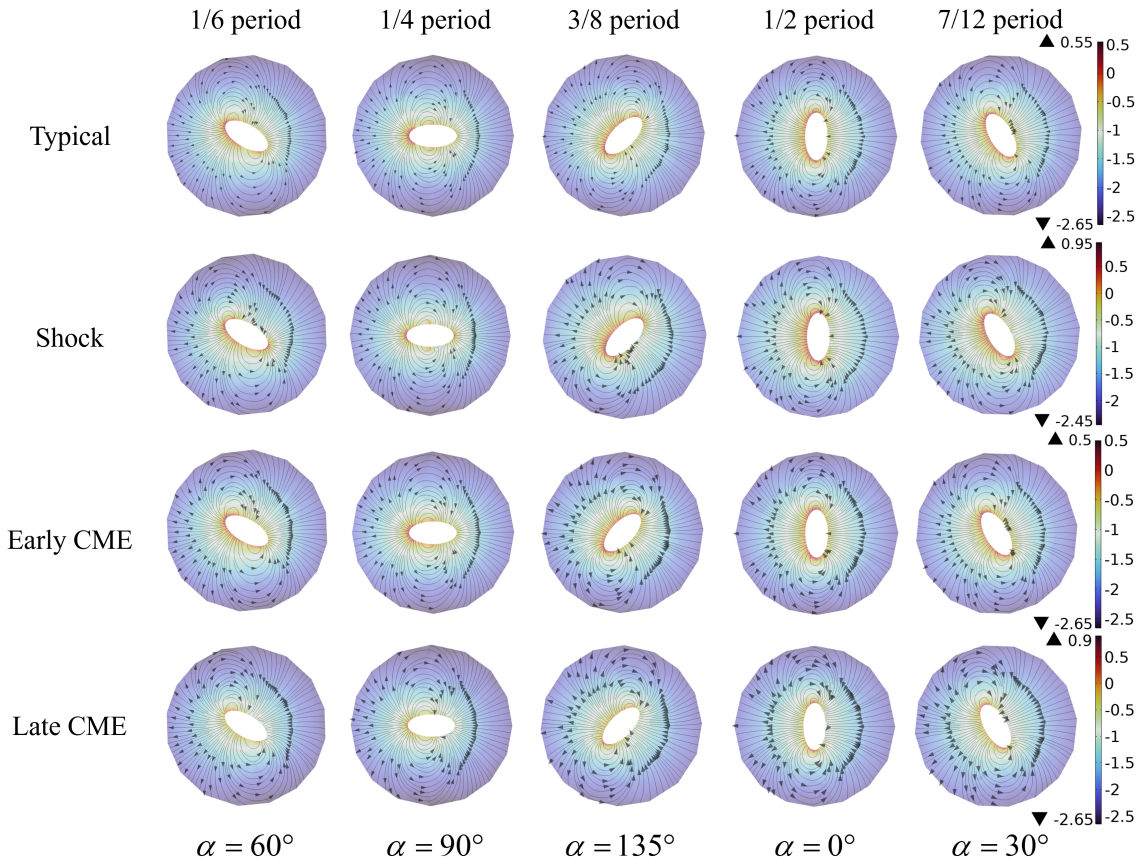


Figure 8. Simulated electric field ($\log_{10}(E_{elef})$) during passage of the modeled CME. The arrows indicate the direction of the electric field lines.

Then we change the rotation period. Charging results of asteroids with varying periods under typical solar wind have been discussed in (1). We now focus on the remaining three conditions. Apart from 0.467 hour, we select three additional periods for each stage based on their respective characteristics, results are shown in Table 4, including the maximum potential V_{\max} , the minimum potential V_{\min} , the maximum electric field strength E_{elef_max} , and the range of potential differences occur on asteroids.

Similar to typical solar wind, asteroids have diminishing V_{\min} as their period grows, this trend can also be seen in V_{\max} , considering it always appears when surrounding plasma is thin, it won't develop to an uncommon value. At the stage shock, asteroid's surface retains a potential difference of over 40V, which does not change with the growth of rotation period, determined that there permanently exists strong electric field strength. Early CMEs are characterized by thin and fast-flowing, making it difficult for electrons and ions to collect near asteroid, the highest average electron density around asteroid is only $1.10e6/m^3$ when period is 1 month. We are only able to identify a 0.008V reduction on the nightside when we obtain a large interval between periods. Conversely, a single hour of period expansion during late CME can lower V_{\min} by 90.35V, together with the conspicuous increasing of ΔV , therefore E_{elef_max} . It should be noted that for slow and dense solar wind, the rotation of asteroid will result in a significant change in surrounding environment, which was overshadowed by electric field migration when we study typical solar wind. At this stage, the minimum potential occurs at $\alpha = 0^\circ$, i.e. $\alpha = 180^\circ$, where asteroid has the largest direct contact area with solar wind, simultaneously owns the widest wake.

(3) Differences between Asteroids with Various Surface Minerals

Results are shown in Figure 9, we select rotation periods of 1 hour, 6 hours and 1 day as representations. Plagioclase is most susceptible to asteroid's rotation period among these minerals, while ilmenite seems indifferent to changes in rotation period, its three potential curves almost overlap. In this respect, orthopyroxene is analogous to plagioclase, as rotation period increases, long-period asteroid's potential is clearly lower.

Table 4. Impact of asteroid's rotation on charging results during various solar storm stages

Stage	Period	V_{\max} (V)	V_{\min} (V)	$E_{\text{elec-max}}$ (V/m)	ΔV (V)
Shock	0.467 hour	16.735	-84.537	12.623	16.701~42.809
	1 hour	16.731	-98.132	13.112	16.393~42.340
	6 hours	16.219	-145.066	14.234	16.150~42.226
	1 day	16.151	-191.032	12.722	16.660~43.209
Early CME	0.467 hour	9.568	-3.729	5.545	12.094~12.906
	1 hour	9.570	-3.755	5.494	12.047~12.910
	12 hours	9.570	-3.755	5.494	12.111~12.910
	1 month	9.568	-3.763	5.428	12.110~12.908
Late CME	0.467 hour	5.615	-73.799	8.717	5.196~18.890
	1 hour	5.626	-111.547	10.638	5.139~23.078
	2 hours	5.413	-179.863	20.347	5.026~34.108
	3 hours	5.433	-270.211	18.802	5.013~48.014

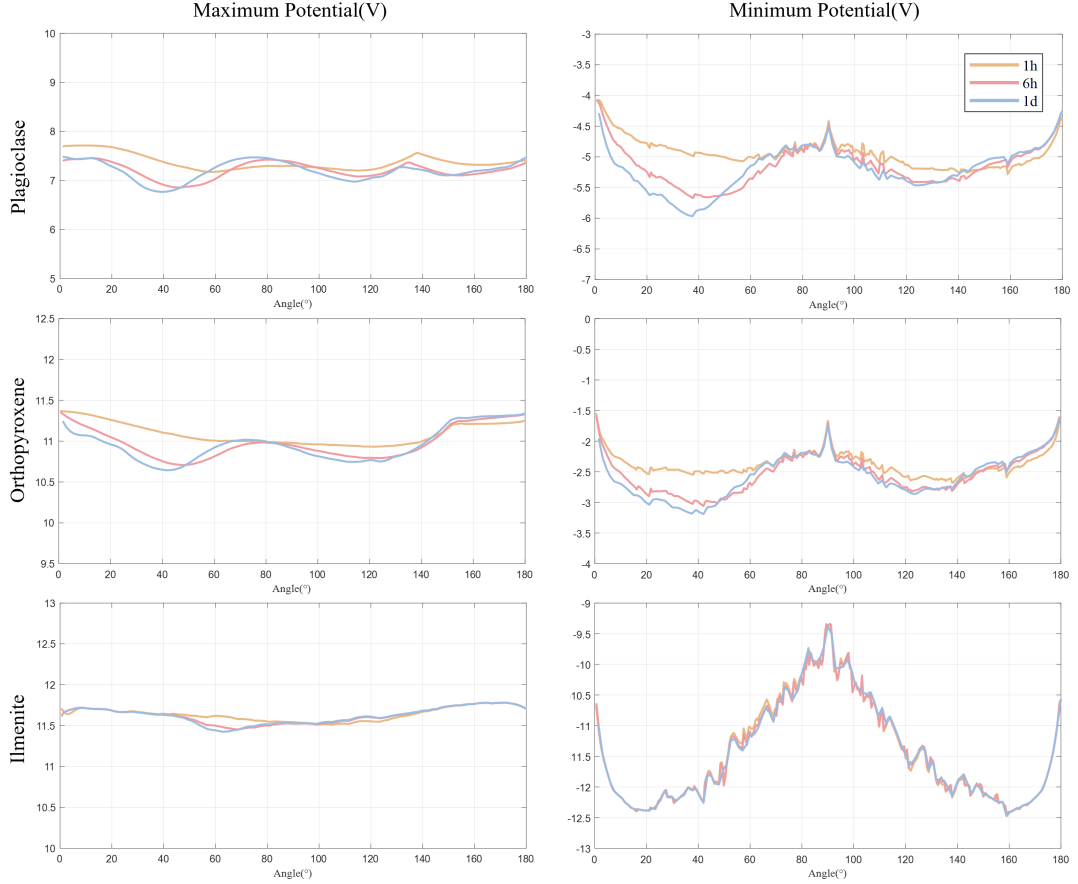


Figure 9. Charging results of three constituent minerals of asteroids. On the left, there are curves showing the maximum surface potential of asteroids composed of three minerals. On the right, corresponding curves depict the minimum potential. All subfigures share a common legend.

About the dayside, we suppose that the intensity of solar radiation stays constant. Cause orthopyroxene and ilmenite have smaller work function than plagioclase, they gain stronger photoelectron currents, which results in a larger and

more stable positive potential at the same time. This stability is improved from top to bottom in Figure 9, along with the decrease of work function.

Granted that there could be a potential difference of 3.1V on the nightside in the absence of CMEs, the impact of the asteroid's attitude on ilmenite is astounding. In contrast, potential of orthopyroxene changes gently, the greatest potential difference product by attitudes can only be 1.58V when rotation period is 1 day, even smaller than that of plagioclase.

5. CONCLUSION

We study how asteroid's rotation effect on its surface charging even surrounding plasma environment under various conditions. A multi-scale modeling method is proposed to implement dynamic three-dimensional simulation, we replace numerical calculation with neural network, improving the efficiency of our research. Rotation periods from 1 hour to half a year are all considered, it is found that rotation period of asteroid can affect its surface potential, specifically, strong electric field will accelerate electrons and ions, then result in higher density and temperature, the change in electrons is much more significant than that of ions, therefore reduce surface potential, until asteroid and plasma reach a dynamic balance, which will be continuously broken and reshaped after rotating. Both potentials on the dayside and nightside will decrease as asteroid's period increases, especially when asteroid rotates to the point where solar wind has an angle of $\alpha = 25 \sim 45^\circ$ with it, the difference in period alone can bring a potential difference of 1V. This trend will gradually slow down with the increasing of period, eventually become stable when period exceeds 1 week, meaning that asteroids with these periods have the ability to reach balance at all angles.

Solar wind parameters and material parameters are also closely related to surface charging. During the passage of solar storm, electron density and ion density become 200 and 10 times that under typical solar wind respectively, potential reached by an asteroid during its rotation can differ by more than 20V, product rapid changes in surrounding plasma, then react to surface potential. Dense and high-temperature plasma can charge asteroid to -84.54V with an electric field of 13V/m, while the potential is -4.78V in normal. As period increasing, asteroids at stage of shock and late CME behaves obvious fluctuations in potential. Different minerals can also exhibit vastly opposed charging results, both plagioclase and orthopyroxene more or less response to changes in rotation period, while ilmenite lacks this sensitivity, its potential mainly depends on the attitude of asteroids.

Our researches provide dynamic simulations of the interaction between solar wind plasma and electric field environments around asteroids, compensate for the lack of consideration in static simulations, namely rotation direction and angular velocity of asteroids. Studies about surface charging phenomenon of asteroids are important for future missions, have general implications in studying the charging properties of other small airless bodies.

1 This work was supported by the National Natural Science Foundation of China (grant No.42241148 and No.51877111).

REFERENCES

- Farrell, W. M., Halekas, J. S., Killen, R. M., et al. 2012, *Journal of Geophysical Research (Planets)*, 117, E00K04, doi: [10.1029/2012JE004070](https://doi.org/10.1029/2012JE004070)
- Ginzburg, V. L. 1970, *The propagation of electromagnetic waves in plasmas*
- Gorin, V. V., Kudryavtsev, A. A., Yao, J., Yuan, C., & Zhou, Z. 2020, *Physics of Plasmas*, 27, 013505, doi: [10.1063/1.5120613](https://doi.org/10.1063/1.5120613)
- Gurevich, A. V. 1978, *Nonlinear phenomena in the ionosphere*, Vol. 10, doi: [10.1007/978-3-642-87649-3](https://doi.org/10.1007/978-3-642-87649-3)
- Halekas, J. S., Delory, G. T., Brain, D. A., et al. 2007, *Geophys. Res. Lett.*, 34, L02111, doi: [10.1029/2006GL028517](https://doi.org/10.1029/2006GL028517)
- Hartzell, C. M., & Scheeres, D. J. 2012, in *2012 IEEE Aerospace Conference*, 1–7, doi: [10.1109/AERO.2012.6187058](https://doi.org/10.1109/AERO.2012.6187058)
- Hastings, D., & Garrett, H. 2004, *Spacecraft-Environment Interactions*
- Hu, P., & Changliang, L. 2018, in *Materials Science and Engineering Conference Series*, Vol. 392, *Materials Science and Engineering Conference Series*, 062180, doi: [10.1088/1757-899X/392/6/062180](https://doi.org/10.1088/1757-899X/392/6/062180)
- Kureshi, R., Tripathi, K. R., & Mishra, S. K. 2020, *Ap&SS*, 365, 23, doi: [10.1007/s10509-020-3740-8](https://doi.org/10.1007/s10509-020-3740-8)
- Li, X., & Scheeres, D. J. 2021, *Icarus*, 357, 114249, doi: <https://doi.org/10.1016/j.icarus.2020.114249>

- Liu, H., Xu, Y., Wang, C., Ding, F., & Xiao, H. 2022, *Materials Research Express*, 9, 025504, doi: [10.1088/2053-1591/ac3a40](https://doi.org/10.1088/2053-1591/ac3a40)
- Novikov, L. S., Mileev, V. N., Krupnikov, K. K., et al. 2008, *Advances in Space Research*, 42, 1307, doi: [10.1016/j.asr.2008.02.019](https://doi.org/10.1016/j.asr.2008.02.019)
- Oudayer, P., Monnin, L., Mateo-Velez, J. C., et al. 2019, *IEEE Transactions on Plasma Science*, 47, 3710, doi: [10.1109/TPS.2019.2919932](https://doi.org/10.1109/TPS.2019.2919932)
- Pandya, A., Mehta, P., & Kothari, N. 2019, *International Journal of Numerical Modelling: Electronic Networks, Devices and Fields*, 32, e2631, doi: <https://doi.org/10.1002/jnm.2631>
- Quan, R., Zhang, C., & Zhang, H. 2023, *IEEE Transactions on Plasma Science*, 51, 1181, doi: [10.1109/TPS.2023.3254516](https://doi.org/10.1109/TPS.2023.3254516)
- Skoug, R. M., Bame, S. J., Feldman, W. C., et al. 1999, *Geophys. Res. Lett.*, 26, 161, doi: [10.1029/1998GL900207](https://doi.org/10.1029/1998GL900207)
- Stubbs, T. J., Farrell, W. M., Halekas, J. S., et al. 2014, *Planet. Space Sci.*, 90, 10, doi: [10.1016/j.pss.2013.07.008](https://doi.org/10.1016/j.pss.2013.07.008)
- Wang, S., Wu, Z.-C., Tang, X.-J., Yi, Z., & Sun, Y.-W. 2016, *IEEE Transactions on Plasma Science*, 44, 289, doi: [10.1109/TPS.2016.2521867](https://doi.org/10.1109/TPS.2016.2521867)
- Whipple, E. C. 1981, *Reports on Progress in Physics*, 44, 1197, doi: [10.1088/0034-4885/44/11/002](https://doi.org/10.1088/0034-4885/44/11/002)
- Xie, L., Li, L., Wang, J., et al. 2023, *ApJ*, 952, 61, doi: [10.3847/1538-4357/acd6ec](https://doi.org/10.3847/1538-4357/acd6ec)
- Xin-Yue, W., Ai-Bing, Z., Tao, J., et al. 2016, *Chinese Journal of Geophysics (in Chinese)*, 59, 3533, doi: [10.6038/cjg20161001](https://doi.org/10.6038/cjg20161001)
- Zimmerman, M. I., Farrell, W. M., Hartzell, C. M., et al. 2016, *Journal of Geophysical Research (Planets)*, 121, 2150, doi: [10.1002/2016JE005049](https://doi.org/10.1002/2016JE005049)
- Zimmerman, M. I., Jackson, T. L., Farrell, W. M., & Stubbs, T. J. 2012, *Journal of Geophysical Research (Planets)*, 117, E00K03, doi: [10.1029/2012JE004094](https://doi.org/10.1029/2012JE004094)